FINAL TECHNICAL REPORT

to the
Office of Naval Research
for

Contract Number N00014-90-J-1528

titled

Low-Frequency Noise Reduction in SQUID Measurements Using Laser Switching

This Final Technical Report
for funding from the
Office of Naval Research
covers the period
January 15, 1990 through January 15, 1992

June, 1992

Blas Cabrera
Principal Investigator

FINAL TECHNICAL REPORT
(January 15, 1990 to January 15, 1992)

(1) **Contract Title:** **Low-Frequency Noise Reduction in SQUID Measurements Using Laser Switching**

Number: **N00014-90-J-1528**

Principal Investigator: B. Cabrera
Physics Department
Stanford University
Stanford, CA 94305
Tel: (415) 723 - 3395

Program Monitor: Dr. Yoon Soo Park

(2) **Technical Objectives:** Reduce SQUID noise in measurements which are intrinsically low frequency or dc. Such low frequency measurements fall below the 1/f knee of the noise energy spectrum and the SQUID performance is degraded substantially below the often quoted white noise levels. We intend to improve the low frequency noise using input circuit modulation at a frequency above the 1/f knee, up-converting the signal in frequency. In our scheme the noise should approach the SQUID white noise floor and the slew rates should approach the original SQUID system slew rate.

(3) **Approach:** Achieve the input circuit modulation using laser switched weak links in superconducting circuits. We modulate an inductance bridge using closely coupled low-inductance superconducting circuits which are opened and closed with laser diodes coupled through optical fibers to modulate the inductance of the arms of the bridge by more than a factor of ten. The bridge acts like a double-pole-double-throw switch which electronically reverses the input coil leads to the SQUID input coil each half cycle.

(4) **Accomplishments:** We have completed our most productive year on this program. Our collaboration with Martin Huber formerly at NIST, Boulder and now on the faculty of the University of Colorado at Denver, has been very successful.

Most importantly, we have demonstrated reduction of the low-frequency noise in an rf SQUID system using double-pole direct switching. Reductions of more than one order of magnitude have been achieved in the SQUID energy noise spectrum. In addition, we have demonstrated the principle of inductive modulation at a modulation depth of 3%.

In understanding the inductive modulation, we have made detailed measurements on the kinetic inductance of a thin-film of niobium (see attached preprint).

We have also developed laser switching technique, for the first time using laser diodes, which avoids trapping of magnetic flux. We can avoid the trapping by using a mechanical shutter with the laser diode. In addition, we have taken advantage of the trapping to study the pinning force on a single trapped vortex in our niobium films (see the attached preprint). This is the first direct measurement of the elementary pinning force that has been reported.

(5) **Significance:** This scheme for the reduction of low frequency noise in SQUID measurements has been demonstrated for both the direct modulation scheme and the inductive modulation scheme, and substantially improves (by more than one order of magnitude in amplitude) the signal to noise in all measurements below the 1/f knee where the noise is currently dominated by SQUID noise.

(6) **Future Efforts:** During the next phase of our program, we will complete the study of the direct switching scheme and develop a high-bandwidth electronics system to take optimum advantage of it. We have requested funding for the purchase of a Quantum Design dc SQUID system which will allow us to investigate the intrinsic noise of the switching scheme at lower levels. We will improve the inductive switching scheme by increasing the modulation depth and we will test thermally stabilized laser diodes to obtain better stability of the switching network. In addition, we will test the switching techniques on YBCO. If the technique is successful, the potential for enormous improvements in the large low-frequency noise of YBCO SQUIDs would materialize.

(7) **Listing:**

(A) **Publications:**

"Low-Frequency Noise Reduction in SQUID Measurements Using a Laser-Driven Superconducting Switch. Part A: Direct Input Circuit Switching", J. T. Anderson, B. Cabrera, M. A. Taber, S. B. Felch and J. Tate, *Rev. Sci. Instrum.* **60**, 202 (1989).

"Low-Frequency Noise Reduction in SQUID Measurements Using a Laser-Driven Superconducting Switch. Part B: Modulated Inductance Switching", J. T. Anderson, B. Cabrera, M. A. Taber, *Rev. Sci. Instrum.* **60**, 209 (1989).

"Low Noise Switching of a Superconducting Circuit by a Laser Induced Weak Link", C. E. Cunningham, B. Cabrera, D. P. Saroff, J. Price and T. Stevenson, *IEEE Trans. on Mag.* **25**, 1022 (1889).

"Demonstration of Absolute Magnetic-Flux Quantization in a Superconducting Circuit", B. Cabrera, C. E. Cunningham and D. P. Saroff, *Phys. Rev. Lett.* **62**, 2040 (1989).

"Correlation of Flux States Generated by Optical Switching of a Superconducting Circuit", C. E. Cunningham, G. S. Park, and B. Cabrera, *Physica* **B** 165&166, 113-4 (1990).

"Vortices Trapped in a Superconducting Microbridge", G. S. Park, C. E. Cunningham, and B. Cabrera, *IEEE Trans. on Mag.* **27**, 3021 (1991).

"Absolute Magnetic Penetration Depth of Thin-Film Niobium Measured by Fluxoid Quantization", C. E. Cunningham, G. S. Park, B. Cabrera, and M. E. Huber, preprint.

"The Laser Switch in SQUID Measurements: Fundamental Experiments and Low-Frequency Noise Reduction", B. Cabrera, proceedings of the IV International Conference on Superconducting and Quantum Effect Devices and their Applications (SQUID'91), in press.

"The Vortex Pinning Force in a Superconducting Niobium Microbridge", G. S. Park, C. E. Cunningham, B. Cabrera, and M. E. Huber, *Phys. Rev. Lett.* **68**, 1920 (1992).

"Modulation Schemes Leading Toward Low-Frequency Noise Reduction in SQUID Magnetometers", C. E. Cunningham, G. S. Park, B. Cabrera, and M. E. Huber, proceedings of the Third Superconductive Electronics Conference.

(7) (B) **Presentations:**

C. E. Cunningham (14 August 1990): " Demonstration of Aharonov- Bohm Effect in a Superconducting Circuit", Conference on Localization, Imperial College, London, England.

C. E. Cunningham (20 August 1990): " Correlation of Flux States Generated by Optical Switching of a Superconducting Circuit", at LT-19, Brighton, England.

George Park (26 September 1990): " Study of a Single Trapped Vortex in a Superconducting Microbridge", at Applied Superconductivity Conference, Snowmass, Colorado.

B. Cabrera (21 June 1991), invited talk: "The Laser Switch in SQUID Measurements: Fundamental Experiments and Low-Frequency Noise Reduction", at the IV International Conference on Superconducting and Quantum Effect Devices and their Applications (SQUID'91), Berlin, Germany.

C. E. Cunningham (27 June 1991), invited talk: "Modulation Schemes Leading Toward Low-Frequency Noise Reduction in SQUID Magnetometers", at the Third Superconductive Electronics Conference, Glasgow, Scotland.

(8) Participants:

B. Cabrera (Principal Investigator)
C. E. Cunningham (Graduate Student)
G. Park (Graduate Student)

M. E. Huber (Assistant Professor at University of Colorado, Denver)

Physica B 165&166 (1990) 113–114
North-Holland

CORRELATION OF FLUX STATES GENERATED BY OPTICAL SWITCHING OF A SUPERCONDUCTING CIRCUIT*

Charles E. CUNNINGHAM, George S. PARK, Blas CABRERA, and Martin E. HUBER §

Physics Department, Stanford University, Stanford, California 94305, USA; § National Institute of Standards and Technology, Electromagnetic Technology Division, Boulder, Colorado 80303, USA

We pulse a superconducting microbridge with light, changing the quantum flux state of a superconducting circuit. Long sequences of pulses are used to measure the degree of correlation between successive flux states. In a series of runs, the pulse length was changed over six decades from 6 ns to 10 ms. The correlations fit a simple Fokker-Planck conditional probability model.

1. INTRODUCTION

We have created a fast, low noise switch using light to drive a superconducting microbridge normal.(1) We plan to use a network of such switches to avoid the 1/f noise in SQUID magnetometers by chopping the input circuit.(2) A switch was connected across the terminals of an rf SQUID for characterization. With the switch open, the magnetic flux in the circuit is arbitrary. With the switch closed, the flux falls into the nearest quantum state, $\phi = n\,\phi_0$, where $\phi_0 = h/2e$ and n is an integer. We noted previously that the correlation between successive flux states was strong with 100 ns pulses and absent with 30 ms pulses.(1) In this experiment, the pulse length was varied over the intermediate range to test a proposed model.

2. EXPERIMENT

The switch (Fig. 1a) is a Nb line 1.5 mm long by 2.2 μm wide by 24 nm thick connecting two Nb contact pads. It is deposited on a sapphire chip (6.3 mm x 6.3 mm x 350 μm). These chips are fabricated at NIST, Boulder using dc sputtering and plasma etching. We make superconducting contact with the chip by compressing dimpled Nb foils against the pads. The foils are spot welded to Nb wires that are connected to an rf SQUID. An optical fiber with a 50 μm core is held directly over the line by a ruby ferrule which is bonded to the chip with epoxy.

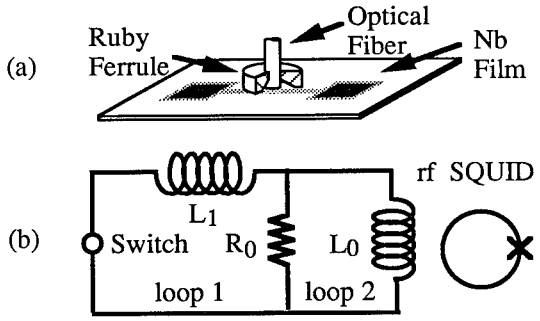

Fig. 1 (a) Laser driven switch. (b) Test circuit for switch. $L_0 = 2.24$ μH, $R_0 \approx 2\ \Omega$, $L_1 \approx 0.4$ μH, $R_{switch} \approx 250\ \Omega$.

The switch is opened by sending 850 nm light from a 2 mW cw laser diode down the fiber. A threshold intensity of about 0.25 $\mu W/\mu m^2$ is necessary to drive the illuminated section of the line normal, opening the switch. Flux can be trapped in metastable pinning sites in the switch, resulting in a nonquantized value of the flux in the circuit. When the switch is superconducting, the laser intensity is biased just below threshold to provide thermal energy which allows flux to detrap. Unfortunately, 50 μW peak-to-peak noise in the laser intensity moves the bias level into and out of the detrapping range during a run.

0921-4526/90/$03.50

Using ^{4}He exchange gas (62 Pa), the chip was heat sunk to a liquid ^{4}He bath. The circuit is surrounded by a Nb shield within a low temperature and high permeability alloy cylinder that attenuates the ambient magnetic field to less than 0.1 μT. The SQUID output is recorded on a digital oscilloscope, and the data is sent to a computer for averaging over 16.7 ms intervals (to remove 60 Hz noise) and for storage.

3. THEORY AND DATA ANALYSIS

The circuit shown in Fig. 1b has two paths for circulating current. Loop 1 has a 1.5 ns time constant (switch normal), and loop 2 has a 1.3 μs time constant. When the switch is normal, the Johnson noise from R_0 can change the flux in either loop no faster than its time constant. Since $L_0 > L_1$, the majority of the magnetic flux is in loop 2. Thus, optical pulses between 1.5 ns and 1.3 μs affect only the relatively small amount of flux in loop 1 and make a small change in the total flux in the circuit.

If the flux in the circuit is ϕ_i before an optical pulse of length t, the probability of finding a flux ϕ_{i+1} in the circuit is given by the solution to the Fokker-Planck equation (3):

$$P(\phi_{i+1},t|\phi_i) \propto \exp\left[-\frac{\{\phi_{i+1}-\phi_i\, e^{-t/\tau}\}^2}{2Lk_BT\{1-e^{-2t/\tau}\}^2}\right], \quad (1)$$

where $\tau = L_0 / R_0$ is the time constant of loop 2 and T is the temperature. For a given set of flux data $\{\phi_i\}$ generated by pulses of length t, Eqn. 1 predicts a point-to-point correlation function:

$$R \equiv \left(\sum_i \phi_i \phi_{i+1}\right)\left(\sum_i \phi_i^2\right)^{-1} = e^{-t/\tau}. \quad (2)$$

We took two data sets of 20 000 flux averages at pulse lengths of 6 ns, 10 ns, 30 ns, 100 ns, 300 ns, 1 μs, 3 μs, 10 μs, 100 μs, 1 ms, and 10 ms. Fig. 2b shows ϕ modulo ϕ_0 plotted over two periods for a typical data set; the SQUID noise is responsible for the finite width to the flux states. For each data set, the flux data were binned as ϕ modulo ϕ_0 and were fit to a Gaussian. In an iterative process known as Chauvenet's criterion (4), the points lying outside 2.5 σ were eliminated and the remaining data were refit until the change in σ was less than 0.1%. We calculated R for each data set and determined the best fit to Eqn. 2 (Fig. 2a).

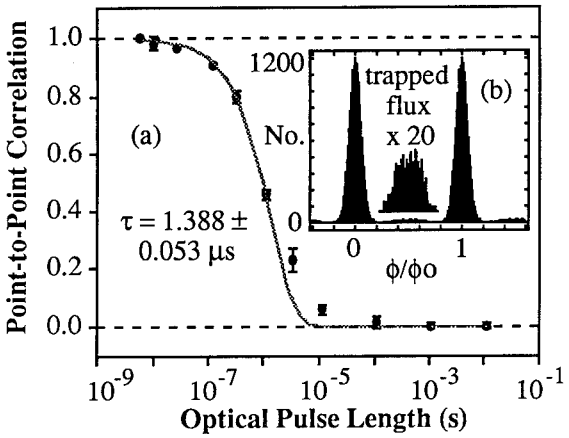

Fig. 2 (a) Point-to-point correlation of flux states with best exponential fit to Eqn. 2. (b) Histogram of 20 000 points of flux data plotted modulo ϕ_0. Inset: trapped flux points magnified x 20.

4. CONCLUSION

The proposed model fits the data well. Theory predicts a time constant of 1.3 ± 0.1 μs, with accuracy limited by the measurement of the shunting resistance R_0. The fit to Eqn. 2 indicates a time constant of 1.388 ± 0.053 μs. The flux trapping appears to be due to the laser diode, as previous operation with a Nd:YAG laser (1,5) did not trap flux. We are now working on the laser stability and, once stabilized, will use the switch to study the intriguing dynamics of the flux trapping process by varying the laser parameters.

ACKNOWLEDGEMENTS

This work was funded in part by the Office of Naval Research, Contract #N00014-87-K-0135.

REFERENCES

(1) Charles E. Cunningham *et al.*, IEEE Trans. Mag. **25** (1989) 1022.
(2) J. T. Anderson *et al.*, Rev. Sci. Instrum. **60** (1989) 202 and 209.
(3) F. Reif: *Fundamentals of Statistical and Thermal Physics* (McGraw-Hill, New York, 1965), pp. 560-582.
(4) H. D. Young: *Statistical Treatment of Experimental Data* (McGraw-Hill, New York, 1962), pp. 78-80.
(5) B. Cabrera, C. E. Cunningham, and D. Saroff, Phys. Rev. Letters **62** (1989) 2040.

The Laser Switch in SQUID Measurements: Fundamental Experiments and Low-Frequency Noise Reduction †

Blas Cabrera

Physics Department, Stanford University
Stanford, California 94305, USA

Low Temperature Physics Group
Preprint Number BC99-91

Physics Department, Stanford University
Stanford, California 94305

June, 1991
revised August, 1991

† Invited talk and paper for SQUID'91, The IV International Conference on Superconducting and Quantum Effect Devices and their Applications, 18-21 June 1991, in Berlin, Germany. This paper will appear in the proceedings.

The Laser Switch in SQUID Measurements: Fundamental Experiments and Low-Frequency Noise Reduction

Blas Cabrera

Physics Department, Stanford University
Stanford, California 94305, USA

Abstract. We are developing a laser-driven superconducting switch. The switch has been used in several fundamental physics experiments which utilize SQUIDs, and in a noise reduction scheme for low-frequency SQUID measurements. The experiments include characterization studies of the laser switch itself, a direct measurement of the pinning force on a single vortex, the measurement of the Cooper pair mass, a study of the Aharonov-Bohm effect, and a measurement of the kinetic inductance of a superconducting thin-film. The noise reduction scheme is based on modulating the input circuit of a SQUID at a frequency above its 1/f knee. The demodulated output is then devoid of the SQUID noise below the modulation frequency. This paper reviews these experiments and reports on their status.

1. The Laser Switch

A number of investigations about the interaction of optical radiation with superconducting microbridges appear in the literature [1], including studies on switching times and relaxation processes. However, the devices described in this paper were the first to utilize the high sensitivity of SQUIDs together with a laser-driven superconducting switch. Using this combination, we have developed new techniques for a number of interesting experiments.

The basic switch (Fig 1) consists of a niobium thin-film microbridge which is illuminated with a laser beam fed through an optical fiber. This fiber is attached to the chip using commercial ruby ferrules which are epoxied to the substrates, typically crystalline silicon or sapphire. We have used two sources for the laser illumination, a 300 mW continuous wave Nd:YAG and several laser diodes.

To characterize the switch performance, we have connected it directly across the input terminals of an rf SQUID [2]. Fig 2a shows a sequence of flux readings taken using the Nd:YAG with a mechanical shutter run in a square wave mode at about 1 Hz. The points along the center of the plot are produced during the laser-on portion of the square wave when the input circuit is open, whereas the wide distribution of quantized points

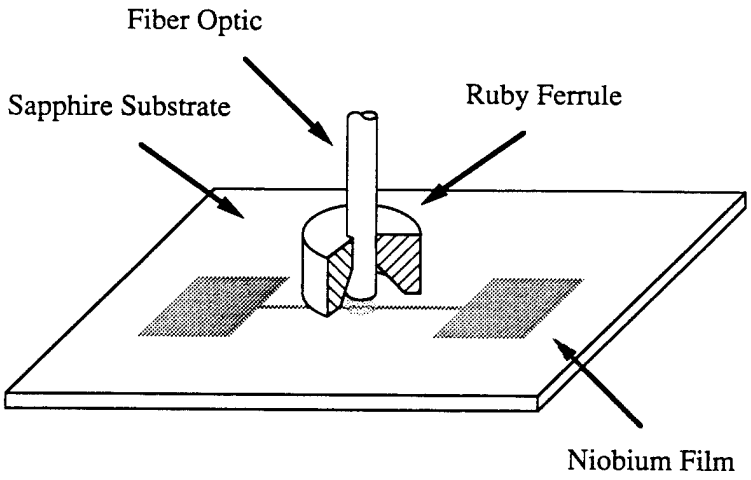

Fig 1 Schematic of laser switch.

corresponds to flux states obtained during the laser-off portion when the quantum coherence is reestablished around the ring. The quantized flux distribution forms a Gaussian which is centered around zero current in the input circuit and has a Boltzmann standard deviation given by $\phi_{rms}^2/2L = kT^*/2$ where L (2 μH) is the inductance of the input circuit and T^*, usually near the T_c of the film, is the freeze-out temperature below which it is very improbable for vortices to move across the microbridge. The position of each point in the distribution is uncorrelated with respect to the position of the previous point.

Next, we use a pulsed laser diode for the the illumination. Now the pulse duration (laser-on) is about 100 ns and again a quantized Gaussian distribution is formed (Fig 2b). However, successive points in the distribution are now strongly correlated, much like a random walk. These correlations are due to the presence of a 3 ohm shunt resistor which is in parallel with the switch across the input of the SQUID. When the switch remains open for times short compared with the $\tau = L/R$ time constant (.75 μs), the shunt resistor acts like a superconducting short, preventing flux from entering the input coil of the SQUID. The distribution of points formed from a set of values immediately following a particular flux state also are Gaussian, but have a narrower standard deviation given by $\phi_{rms}^2 = LkT^*(1 - e^{-2t/\tau})^2$. The centroid of this distribution is near the previous flux state, but shifted toward the zero current position. These properties are described by the conditional probability function [2]

$$P(\phi_{i+1},t;\phi_i) \propto \exp\left(- \frac{(\phi_{i+1} - \phi_i\, e^{-t/\tau})^2}{2LkT^*(1 - e^{-2t/\tau})^2} \right).$$

We performed a careful study of the fit of our data to this function for a range of pulse times from 6 ns to 100 ms. The data fit the function well (Fig 3) and convincingly set an upper limit on the switching times of <6 ns. The thermal relaxation time constant for these films is ≈ 1 ns.

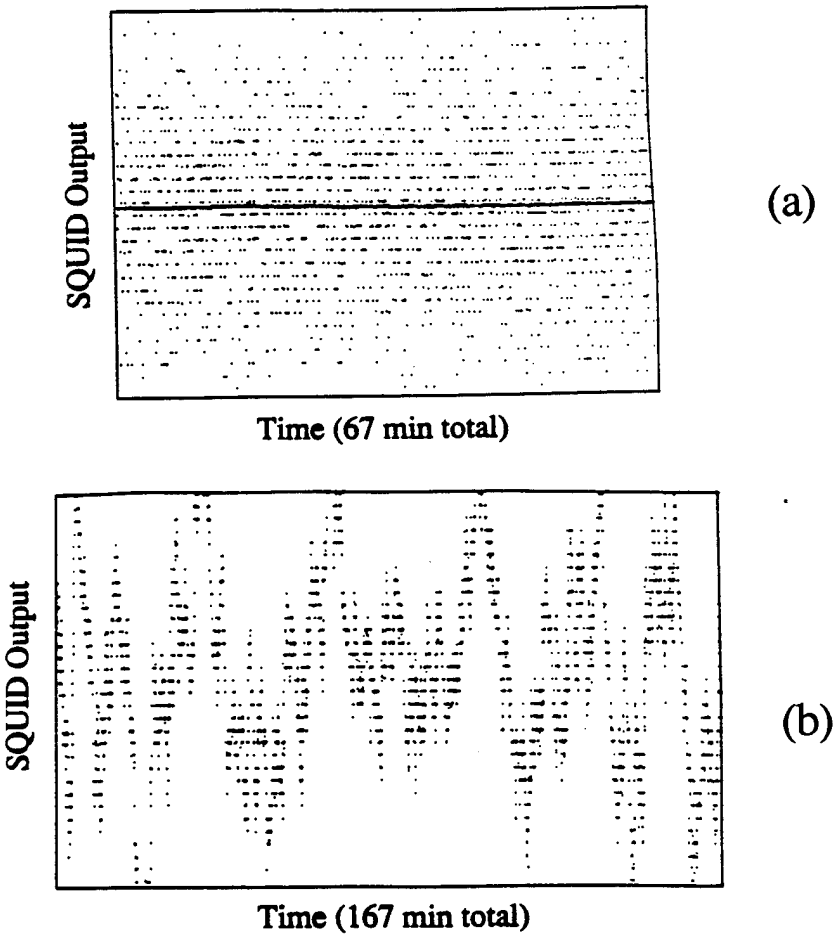

Fig 2 Evolution of flux quantum states (a) using a Nd:YAG laser, and (b) using a laser diode.

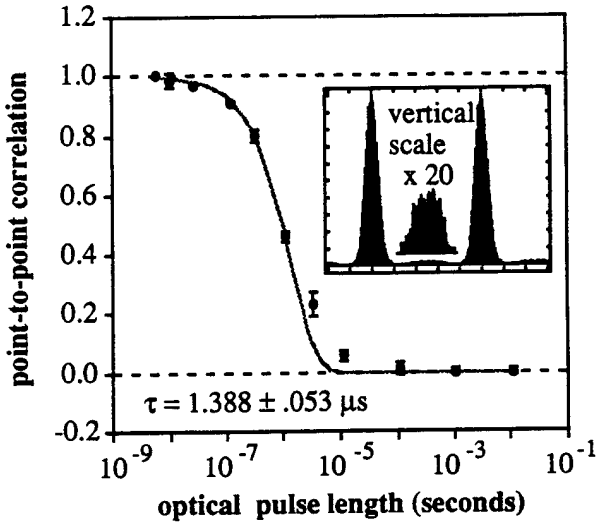

Fig 3 Fit of data to conditional probability function.

One final point about the switch operation is that in looking closely at the distribution from the laser diode data (Fig 2b), we find non-quantized flux points which occur about 5% of the time. These correspond to a vortex which is trapped right in the area of the film which was illuminated by the laser. The apparent fractional value in the flux is due to the superposition of two different flux quantum states on opposite sides of the vortex, and its value between the two states is roughly proportional to the position of the vortex along a direction perpendicular to its length. Next, we will utilize this feature to study the vortex pinning force.

2. Vortex Pinning Force

Very recently, we have taken advantage of the flux trapping as a tool to measure the pinning force on a single vortex [3]. We repeatedly open and close the laser switch until a fractional flux value is obtained. Then, we run a current through the 2 μm wide niobium line until the vortex moves to the edge of film, usually all at once, but sometimes in two steps indicating that it fell into a deeper pinning site on its way to the edge and a larger current was needed to free it. The circuit which provides the current has two branches, the first is connected in parallel with the switch and the second is inductively coupled to the SQUID input circuit. An adjustable bridge proportions the drive current in such a way that the SQUID output remains

constant unless the vortex moves. Using this technique, we have measured single-vortex pinning forces in the range of 10^{-4} N/m for our 20 nm thick Nb films.

We plan to extend the technique in two ways. First we will use a dc SQUID to improve the signal-to-noise by more than an order of magnitude. With this increased sensitivity, we will examine the elastic region where the vortex moves in its pinning potential but does not escape. It will then be possible to map out the shape of the pinning potential. Second, we will attempt to utilize the technique on high temperature superconductor films such as YBCO. The technique will work, unless we trap many vortices each time we operate the switch. We have been very encouraged by the initial results with low T_c films and feel that this technique will be very useful in pinning studies.

3. Cooper Pair Mass

Originally, we developed the laser switch for an experiment to determine the mass of a Cooper pair [4]. The mass m* is defined through the quantum mechanical relation $m^*\mathbf{v} = (h/2\pi)\,\mathbf{grad}\,\phi - e^*/c\,\mathbf{A}$, where $\mathbf{v}$ is the superfluid velocity and ϕ the phase of the order parameter. For a bulk superconductor at rest in the laboratory, $\mathbf{v}=0$ in the interior so no information can be obtained about m*. In fact it is necessary for $\mathbf{curl}\ \mathbf{v} \neq 0$ around a closed path. This condition is easily achieved using a rotating superconductor. From the gauge invariant relation above, it can be shown that the interior of a rotating superconductor contains a uniform field proportional to the angular velocity ω. This field, $B_L = 2m^*c/e^*\ \omega$ is called the London field.

If we now consider a rotating ring, we can measure this London magnetic flux in terms of the flux quantum $\phi_0 = hc/e^*$. The total flux measured by a stationary pick up loop connected to a SQUID is given by $\phi = n\,\phi_0 - (2m^*c/e^*)\,\omega\cdot\mathbf{S}$ where $\mathbf{S}$ is the area bounded by the ring. This equation corresponds to a set of parallel lines (see data in Fig 4) which are separated by ϕ_0 along the ϕ axis and by $\Delta\omega$ along the frequency axis. Looking at the equation, we see that $h/m^* = 2\,\Delta\omega\,S$. Thus by measuring $\Delta\omega$ and the area S to high precision, we obtain a direct measure of h/m^*. We have made such a measurement with a statistical accuracy of 5 ppm and a systematic uncertainty of 20 ppm.

Measuring an area to such precision required depositing a thin-film superconducting line on the equator of a precision quartz hemisphere, and using laser interferometric methods to measure the equatorial area [4]. The precision for the $\Delta\omega$ determination is made by sweeping the spin speed through about 1000 null crossings. Fig 4 shows a slow spin ramp through 0.5 Hz change. Each point is taken after the coherence of the ring is broken and reestablished using a laser switch positioned to shine on the

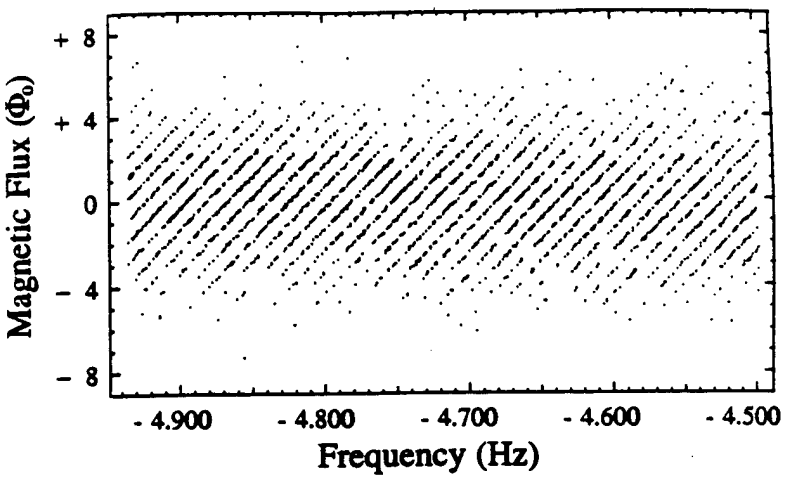

Fig 4 Flux quantum data during slow ramp of spin speed.

line. Without the switch we would always remain on the same line and be unable to measure the frequency shift between lines. As with Fig 2a, the distribution of data points along the ϕ axis forms a Gaussian centered around zero current in the ring. Now however, the flux quantum states are tilted due to the additional phase shift of the order parameter produced by the rotation.

Our result for m', the Cooper pair mass with relativistic corrections added is $(m'/2m_e)_{exp}$ = 1.000 084 (5) (20). Thus a Cooper pair has very nearly the mass of two free electrons at rest. However, several calculations suggest that $(m'/2m_e)_{theo}$ = 0.999 992 (4), not only smaller in magnitude, but also on the other side of unity. Interestingly, the relativistic corrections contain a kinetic energy and a potential energy term, with $\langle T\rangle/2m_ec^2$ = + 0.000 180 and $\langle V\rangle/2m_ec^2$ = - 0.000 188, such that $(m'/2m_e)_{theo} = 1+[\langle T\rangle+\langle V\rangle]/2m_ec^2$. Our measurement suggests that a complete relativistic treatment might result in $m'/2m_e = 1+[\langle T\rangle+{}^1/_2\langle V\rangle]/2m_ec^2$ = 1.000 086. A more detailed calculation needs to be performed which includes all first-order relativistic effects in a self-consistent formalism. We also plan to improve the measurements.

4. Absolute Aharonov-Bohm Effect

Our experiment to measure the absolute significance of the magnetic vector potential [5] was motivated by a suggestion that the absolute magnetic flux through superconducting circuits might contain a fractional residue [6]. In this theory, flux quantization through a superconducting circuit would take the form $\int \mathbf{A}\cdot d\mathbf{l} = (n+r)\,\phi_0$ where n is an integer and $0<r<1$ is a residue.

The superconducting circuit would trap r at the time the global phase coherence was first established around the circuit. Subsequent changes in the flux threading the circuit, which arise from vortices passing through a Josephson junction or across a microbridge, would change n but not r, since the local phase coherence is always maintained in such microscopic processes with dimensions smaller than the coherence length of the superconductor.

In order to test for the possibility of fractional flux quantization, it was necessary to devise an experimental technique for completely destroying and reestablishing the phase coherence over distances much greater than the coherence length. Repeatedly heating a portion of a macroscopic superconducting circuit does not generate a quantized flux distribution because vortices are trapped in various portions of the superconducting material making up the circuit. Since the locations of these vortices change after each cooling, a continuum of flux values is seen in measurements.

Our laser switch circumvented these experimental difficulties and allowed for the first time a sensitive test of the fractional flux quantization theory. Fig 5a shows a schematic representation of the experiment. The optically switched element is connected directly across the input coil of an rf SQUID sensor. In addition, the circuit threads a toroidal solenoid (Fig 5b) enclosed in a superconducting shield which can couple flux to the circuit while shielding all portions of the superconducting material from the magnetic field. The shield geometry is not a closed toroid, which would prevent any changes in the magnetic flux coupling to the circuit, but rather there is a long overlap region which is electrically isolated.

To test the absolute nature of the Aharonov-Bohm effect, a slowly changing magnetic flux was introduced through the circuit using the toroidal solenoid. Data were taken before, during, and after the ramping (Fig 5c). The centroid of the distribution remains at zero current (as in Fig 2). To calibrate the slope of the ramp portion, an identical run was performed with the laser intensity turned down so that the switch remained superconducting throughout. These data are superimposed with no dc offset and show that the slopes are the same for the two runs.

To within the experimental uncertainty of about 1%, these SQUID-based data show that flux changes made by a toroidal solenoid when the circuit is open and without global phase coherence are always accounted for in full when the circuit is later allowed to return to the phase-coherent quantum state. There was no evidence for fractional flux quantization in superconducting circuit and the data are completely consistent with the absolute significance of the magnetic vector potential in conventional quantum mechanics.

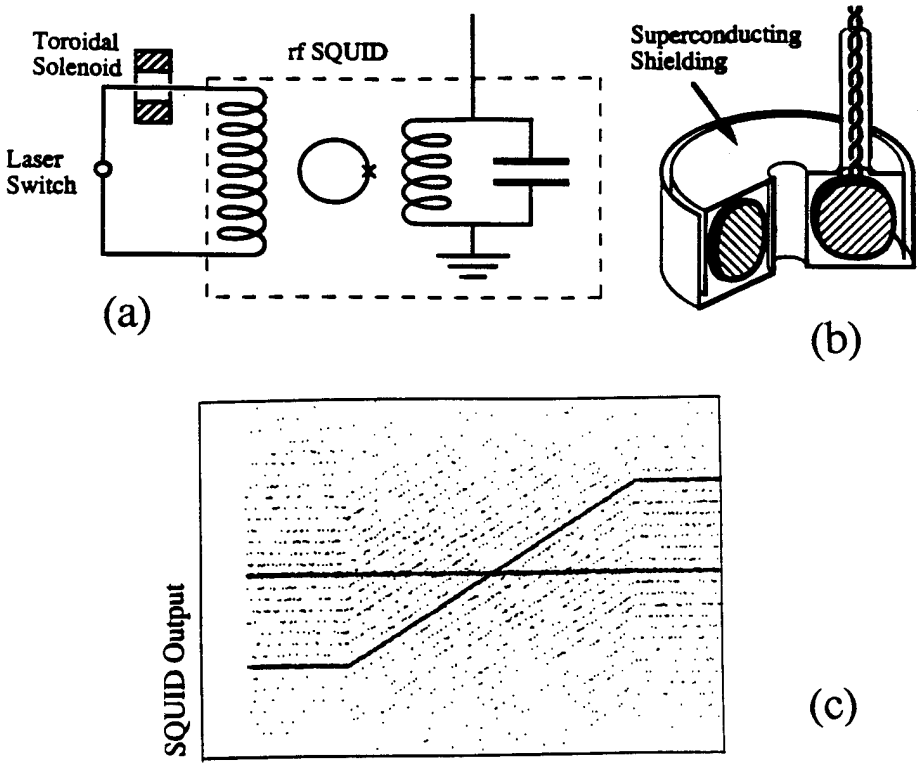

Fig 5. (a) Schematic of superconducting circuit with laser switch and (b) toroidal solenoid. (c) Data run with ramped solenoid current and a superimposed run with the switch superconducting throughout.

5. Kinetic Inductance

We have recently completed a detailed study of the kinetic inductance of a thin-film circuit, measuring both its absolute value and its temperature dependence [7]. We find excellent agreement with the predictions of BCS theory in the dirty limit [8].

The inductance of a superconductor has two parts, one due to the magnetic field and the other due to the momentum of the current carriers.

These can be derived from the fluxoid quantization condition $\phi + (4\pi/c)\lambda^2 \int j_s \cdot dl = n\,\phi_0$ where ϕ is the magnetic flux threading the loop and j_s is the supercurrent density. We can further obtain a lumped parameter equation by integrating over the cross-sectional area of the wire, so that j_s becomes the total current I. Then $L_M I + L_K I = n\,\phi_0$, where L_M is the magnetic inductance and L_K the kinetic inductance. For a wire with thickness t and width w both small compared to λ, the current density is approximately uniform across the wire and the kinetic inductance has the simple form $L_K = \mu_0 \lambda^2 l/wt$ where l is the length of the circuit. We have transformed from cgs to SI units so that L_K can be easily compared with L_M in henry.

The circuit shown in Fig 6a is patterned from a single 11 nm thick niobium film on a silicon substrate. It consists of a 1 mm square loop which can be interrupted with the laser switch and a 20.5 turn inductively coupled coil which surrounds the square loop. This coil is directly connected to the input circuit of the SQUID after passing through a toroidal solenoid which is used to change the applied flux through the circuit.

Having previously determined the inductance of the SQUID input inductor to be 2.24 μH, the measurement of the total inductance of the square loop is made utilizing three measurements. First the response of the SQUID to a ramped current in the solenoid is measured with the square loop normal. Second the measurement is repeated with the loop superconducting. Finally, a distribution of quantized flux levels is measured in the loop by repeatedly opening and closing switch and the response to a 1 ϕ_0 change is determined. These three independent measurements allow L_2, L_1, and M to be determined. The procedure is repeated over the range of temperatures allowed by the SQUID.

The results for the total inductance of the square loop are plotted in Fig 6b. Also shown is the best fit for the magnetic inductance which is very nearly temperature independent and kinetic inductance which diverges as the temperature approaches the critical temperature. However, the divergence from the BCS dirty limit is significantly slower than the phenomenological relation $1/(1-(T/T_c)^4)$ which is approximately correct for the clean limit but should not be used for this case. A better phenomenological relation is $1/(1-(T/T_c)^4)^{3/2}$. The best fit parameters for the BCS dirty limit are L_{2M} = 5.4 +/- 0.3 nH, $L_{2K}(0)$ = 3.3 +/- 0.2 nH and $\lambda(0)$ = 127 +/- 9 nm, whereas the no free parameter calculated values are L_{2M} = 5.8 +/- 0.1 nH, $L_{2K}(0)$ = 3.1 +/- 0.4, and $\lambda(0)$ = 122 +/- 1 nm. We consider this fit to be excellent and the greatest source of error is due to the uncertainty in the film thickness (11 +/- 1.5 nm).

Note that these values for λ are about 50% larger than usually quoted for Nb films because below about 20 nm in thickness, the resistivity increases and the transition temperature decreases. Also note that for the BCS dirty limit the kinetic inductance can be written as $L_K(0) = (h/2\pi^2) R/\Delta$, which depends only on the normal state resistance R and T_c, through $\Delta = 1.76\,kT_c$, and is independent of film thickness and coherence length.

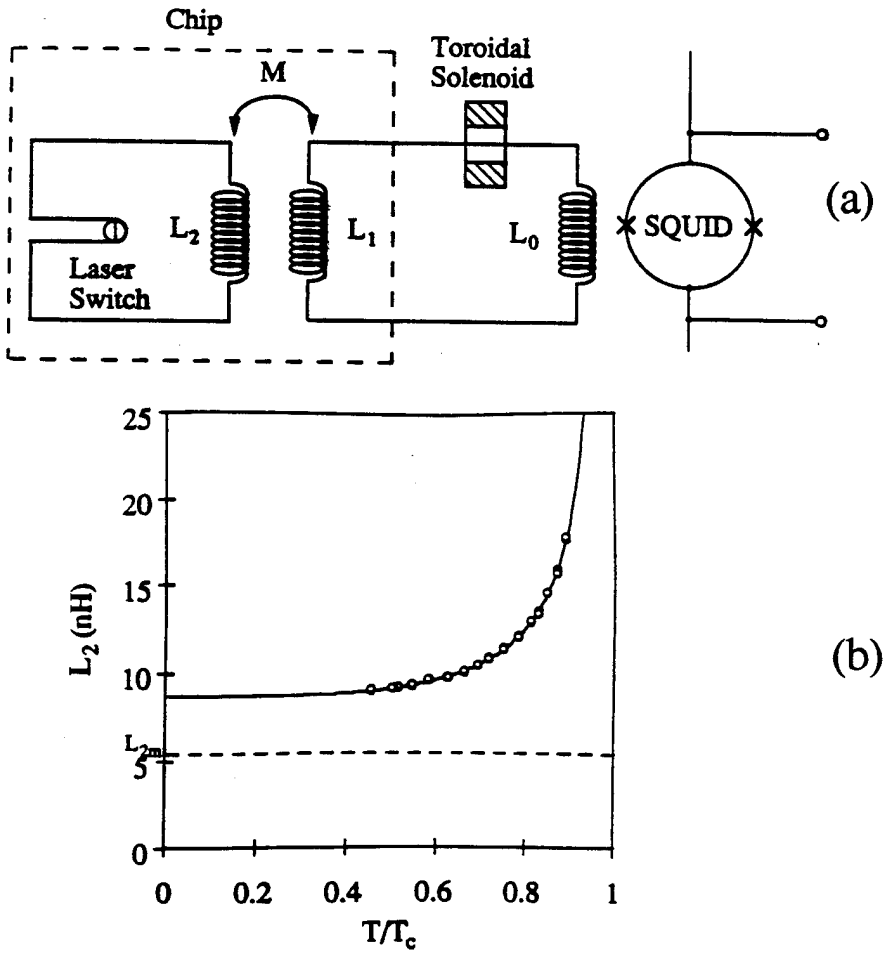

Fig 6 (a) Schematic of kinetic inductance measurement circuit.
(b) Calculated and measured inductance of square loop.

6. Reducing Low-Frequency Noise

In the previous sections, we have discussed a number of SQUID-based fundamental experiments. In all of them, we were forced to use the SQUID at low-frequencies, where the 1/f noise dominates the energy noise spectrum. Much progress has been made on reducing the 1/f noise in dc SQUIDs by making better junctions and by using bias current modulation [9]. However, that technique does not remove the so-called flux noise. In addition, the design for the lowest white noise SQUID, utilizing submicron junctions, often have worse 1/f noise. Instead, we are developing an input

coil circuit modulation scheme which is an add-on component between the pickup coil and the SQUID input coil [10].

Fig 7a shows a schematic of the chopping idea. To demonstrate the idea, we have adapted the same circuit used to measure the kinetic inductance to modulate the SQUID input circuit. Unfortunately, only a 3.5% modulation depth is produced, but the experiment demonstrates improved low-noise performance and proof-of-principle.

Fig 7b shows the noise energy spectral density for our rf SQUID including the 1/f portion (solid line). By forming the difference output between the laser switch on and off SQUID output, we obtain the upper spectral density. Its white noise is $(1/.035)^2 \approx 1000$ times higher, but the low frequency noise is actually lower in the hashed region. We are currently developing a design which uses a dc-SQUID-style washer coil, we expect to obtain modulation depths of over 50%.

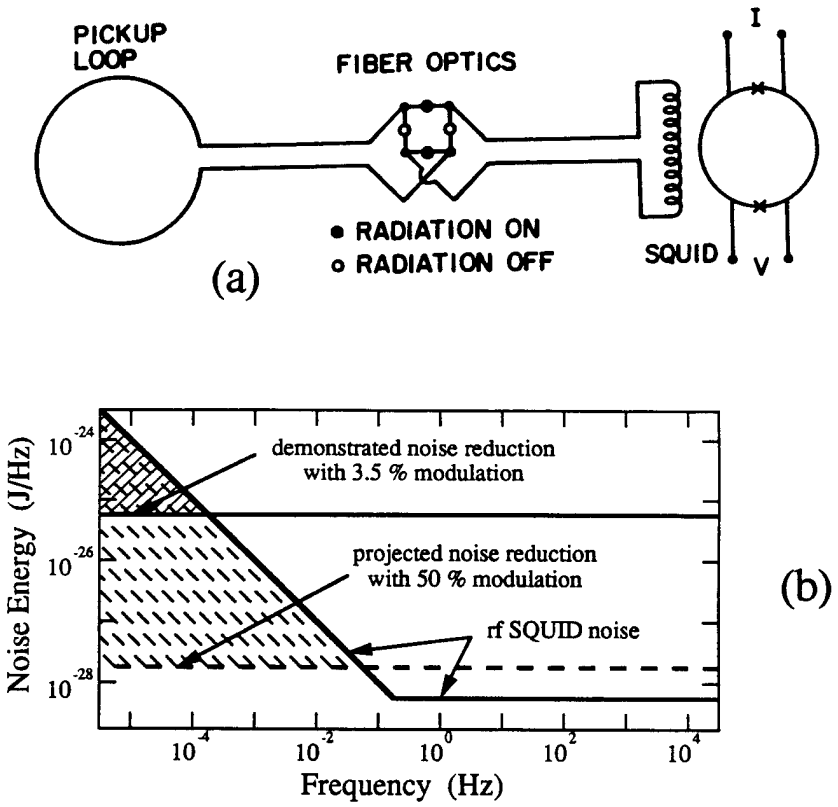

Fig 7 (a) Schematic of input circuit modulation. (b) Noise energy spectra from demonstration run with chip in Fig 6a.

7. Conclusions and Acknowledgements

These experiments have demonstrated several interesting techniques utilizing the laser switch in SQUID measurements, and we are confident that these will continue to improve and others will be developed. The low noise reduction scheme has been shown to work, and is a promising way to significantly improve low-frequency or dc SQUID measurements.

The experiments described in this paper were performed by a number of students and colleagues. These include C. E. Cunningham and G. Park currently at Stanford, D. P. Saroff currently at NASA-Ames Research Center, J. Tate and D. McIntyre currently at Oregon State University, J. T. Anderson currently at Hewlett-Packard, and M. Huber currently at University of Colorado at Denver. This research was funded in part by ONR Contracts N00014-87-K-0135 & N00014-90-J-1528, and NSF Grant DMR 84-05384.

References

[1] L. R. Testardi, *Phys. Rev.* **B4**, 2189 (1971); J. A. Pals, K. Weiss, P. M. T. M. van Attekum, R. E. Horstman, and J. Wolter, *Phys. Rep.* **89**, 323 (1982); and E. M. Gershenzon, M. E. Gershenzon, G. N. Gol'tsman, A. D. Semenov, and A. V. Sergeev. *Sov. Phys. JETP* **59**, 442 (1984).

[2] C. E. Cunningham, G. S. Park, B. Cabrera and M. E. Huber, *Physica* **B165**, 113 (1990).

[3] G. S. Park, C. E. Cunningham, B. Cabrera and M. E. Huber, Stanford Low Temperature Group Preprint BC101-91.

[4] J. Tate, B. Cabrera, S. B. Felch, and J. T. Anderson, *Phys. Rev. Lett.* **62**, 845 (1989).

[5] B. Cabrera, C. E. Cunningham, and D. Saroff, *Phys. Rev. Lett.* **62**, 2040 (1989).

[6] J. Q. Liang and X. X. Ding, *Phys. Rev. Lett.* 60, 836 (1988).

[7] C. E. Cunningham, G. S. Park, B. Cabrera and M. E. Huber, Stanford Low Temperature Group Preprint BC98-91.

[8] P. B. Miller, *Phys. Rev.* **113**, 1209 (1959)

[9] V. Foglietti, W. J. Gallagher, and R. H. Koch , I*EEE Trans. Magnet.*, **Mag-23**, 1150 (1987).

[10] J. T. Anderson, B. Cabrera, M. A. Taber, S. B. Felch, and J. Tate, *Rev. Sci. Instrum.* **60**, 202 (1989); J. T. Anderson, B. Cabrera, and M. A. Taber, *Rev. Sci. Instrum.* **60**, 209 (1989); and C. E. Cunningham, G. S. Park, B. Cabrera and M. E. Huber, in preparation.

FIGURE CAPTIONS

Fig 1 Schematic of laser switch.

Fig 2 Evolution of flux quantum states (a) using a Nd:YAG laser, and (b) using a laser diode.

Fig 3 Fit of data to conditional probability function.

Fig 4 Flux quantum data during slow ramp of spin speed.

Fig 5. (a) Schematic of superconducting circuit with laser switch and (b) toroidal solenoid. (c) Data run with ramped solenoid current and a superimposed run with the switch superconducting throughout.

Fig 6 (a) Schematic of kinetic inductance measurement circuit. (b) Calculated and measured inductance of square loop.

Fig 7 (a) Schematic of input circuit modulation. (b) Noise energy spectra from demonstration run with inductance modulation chip in Fig 6a.

T-MAG/27/2/8/44138

Trapped Vortices in a Superconducting Microbridge*

George S. Park
Charles E. Cunningham
Blas Cabrera
Martin E. Huber

Reprinted from
IEEE TRANSACTIONS ON MAGNETICS
Vol. 27, No. 2, March 1991

TRAPPED VORTICES IN A SUPERCONDUCTING MICROBRIDGE*

George S. Park, Charles E. Cunningham, Blas Cabrera
Physics Department, Stanford University
Stanford, Ca 94305

Martin E. Huber
National Institute of Standards and Technology
Electromagnetic Technology Division
Boulder, Co 80303

Abstract

Laser light pulsed onto a Nb microbridge drives it momentarily normal and changes the quantum flux state of a superconducting inductive loop. The flux state is measured by a SQUID coupled to the loop. With a Nd:YAG laser, vortices are never trapped in the microbridge; with a diode laser, vortices are sometimes trapped. The spatial distribution of the trapped flux was studied. The effect of the optical pulse fall time on the frequency of flux trapping was found to be unimportant from 200 ns to 8 ms. Noise spectrum analysis indicates that the laser diode is 5 to 25 times noisier than the Nd:YAG laser at the characteristic frequency of the loop. This noise is believed to be responsible for flux trapping in the microbridge.

Introduction

We are testing a fast, low-noise switch for use in a chopping network to reduce the 1/f noise in SQUID magnetometers. Our switch is a superconducting microbridge which is driven normal through photon-electron interactions.[1] The film remains below its thermodynamic transition temperature, and the resistance of the switch follows the optical power on a nanosecond timescale.[2] The microbridge is repeatedly pulsed with laser light. The thermal energy at the switch and the inductance of the superconducting loop are large enough that

$$\frac{\phi_0^2}{2L} << \frac{k_B T}{2}, \qquad (1)$$

so the system can fall into any of several quantum states $\phi = n\,\phi_0$, where $\phi_0 = h/2e$ is the flux quantum of superconductivity and n is an integer. With light from a shuttered Nd:YAG laser, the system always falls into a quantized flux state. With a current modulated diode laser, however, flux is occasionally trapped in the microbridge, which is detected as a nonquantized flux state. As flux trapping would increase significantly the noise in our modulation scheme, it is important to determine the conditions under which flux is trapped.

Experiment

The switch (Fig. 1) is a meandering Nb line 2.2 μm wide and 24 nm thick connecting two Nb contact pads. The meander has a 5 μm pitch and occupies a 70 μm by 70 μm square. This pattern is deposited on a sapphire chip (6.3 mm by 6.3 mm by 350 μm), and a passivating 1 μm layer of SiO is deposited over the entire chip except at the pad areas. These chips are fabricated at NIST, Boulder, using dc sputtering and plasma etching. We make superconducting contact with the chip by compressing dimpled Nb foils against the pads. The foils are spot welded to Nb wires that are connected to an rf SQUID. An optical fiber with a 50 μm core is held directly over the meander square by a ruby ferrule epoxied to the chip (Fig. 2).

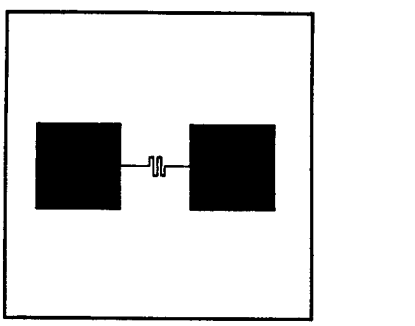

Figure 1. Optical switch chip. The meander is not drawn to scale.

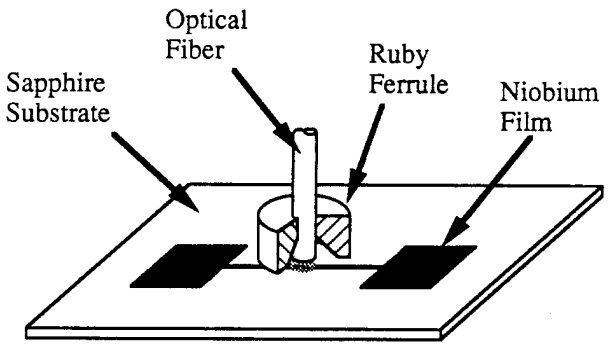

Figure 2. Positioning of the optical fiber over the meander.

The chip and the SQUID are set in an epoxy fiberglass housing surrounded by a Nb shield. This assembly is placed within a low temperature, high permeability alloy cylinder that attenuates the ambient magnetic field to less than 0.1 μT. The assembly is heat sunk to a liquid He bath using He exchange gas at 62 Pa (0.8 torr) for thermal coupling.

The switch is opened by sending laser light down the fiber from either a Nd:YAG or GaAlAs diode laser. A threshold intensity of about 0.25 $\mu W/\mu m^2$ is necessary to drive the illuminated section of the microbridge normal, opening the switch. The 1.06 μm light from the Nd:YAG laser is modulated with a shutter (0.5 ms closing time), and the 850 nm light from the diode laser is modulated by changing the diode current. The laser intensity is monitored by a photodiode receiving 8% of the laser light.

The SQUID output is sent through an antialiasing filter to a digital oscilloscope. A computer reads these data and averages them over an integer multiple of 16.7 ms (to remove 60 Hz noise).

Theory

As the switch becomes superconductive, the loop falls into the nearest quantum flux state which satisfies Eq 2.

$$\phi + \lambda^2 \mu_0 \oint \vec{j}_s \cdot \vec{dl} = n\,\phi_0\,, \qquad (2)$$

where λ is the London penetration depth of the superconductor, φ is the magnetic flux threading the integration path, j_s is the supercurrent density, and n is an integer (constant for all integration paths). During the superconductive transition, this process may go awry if flux in the microbridge gets trapped in a metastable pinning site. In that case, Eq 2 becomes

$$\phi + \lambda^2 \mu_0 \oint \vec{j}_s \cdot \vec{dl} = \begin{pmatrix} n \\ n \pm 1 \end{pmatrix} \phi_0 \quad \begin{pmatrix} \text{above vortex} \\ \text{below vortex} \end{pmatrix}, \qquad (3)$$

*Contribution of the U.S. Government, not subject to copyright.

Manuscript received September 24, 1990.

with different quantization conditions for integration paths around the loop which pass above and below the vortex (Fig. 3). This results in a measured value of the magnetic flux modulo ϕ_0 which lies between quantized flux states.

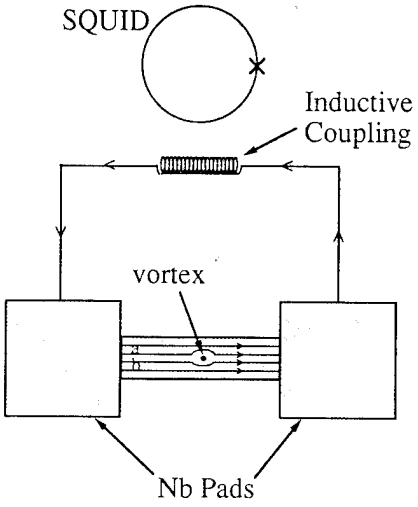

Figure 3. Integration paths (a) above and (b) below vortex.

We calculated the circulating current generated by a trapped vortex at various positions in the microbridge. For simplicity, the problem is made one-dimensional by stretching the core of the vortex into a line containing the same amount of magnetic flux at the same distance from the edge of the microbridge. In one model, the loop is treated as concentric filamentary rings (Fig. 4a); in the other, it is treated as parallel filaments attached to a bulk inductor (Fig. 4b). The magnetic flux penetrates the superconductor between filaments. The loop reacts to the vortex by generating a current distribution determined by the quantization condition, Eq 3, which may be rewritten for the filaments as:

$$\sum_b \left(M_{a\,b} + \delta_{a\,b}\, L_K\right) I_b = \begin{cases} \phi_0 & (a < a_{vortex}) \\ 0 & (a > a_{vortex}) \end{cases}, \qquad (4)$$

where M_{ab} is the mutual inductance matrix and L_K is the kinetic inductance of the filament. By inverting Eq 4, the filamentary currents are calculated. They are summed to obtain the extra current which couples to the SQUID due to the vortex. As is shown in Fig. 5, a trapped vortex results in a measured value of the flux modulo ϕ_0 which is related to the physical position of the pinning site in the microbridge.

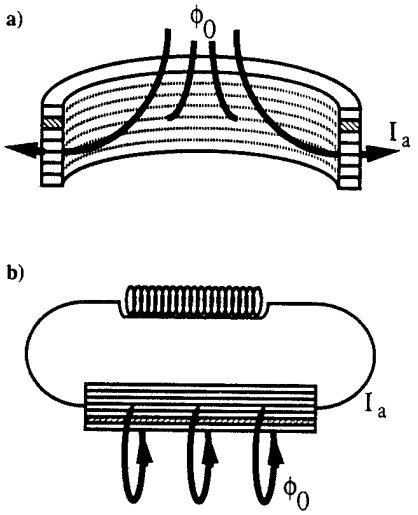

Figure 4. (a) Concentric ring model and (b) Parallel filament model of trapped flux.

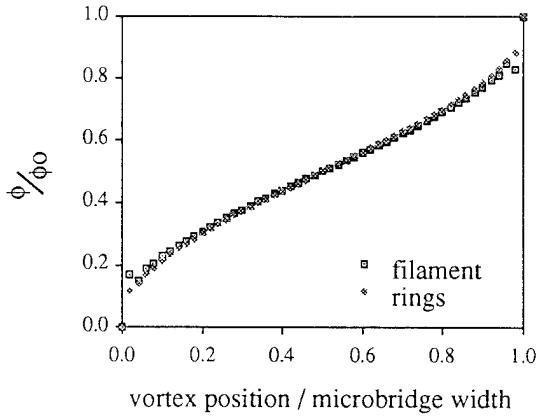

Figure 5. Fractional flux coupled to the SQUID due to the vortex. The two models are in good agreement except at the edges, where the large current gradient causes the discrete model to break down.

Impurities and thin spots in a superconducting microbridge form pinning sites. The measured distribution of trapped flux depends on the depth of the pinning sites relative to the available thermal energy as the microbridge cools. With a deep pinning site, the vortex has insufficient thermal energy to escape and is always trapped at the same place. As the noise due to flux motion in the pinning site is much less than the SQUID noise, the width of the distribution of flux in a deep pinning site equals that of the distribution in the quantized state.

If there is no deep pinning site, the vortex can be trapped in one of the many shallow sites. As the microbridge cools, the vortex has enough thermal energy to hop between sites. Fig. 6 shows the energy of a vortex in a microbridge with no pinning sites.[3] The vortex feels an expulsion force proportional to the gradient of its energy. Where the gradient is large (near the edges), the expulsion force exceeds the pinning force, and the vortex can escape. Where the gradient is small (near the middle), the expulsion force is less than the pinning force, and the vortex will be trapped. The measured distribution is the sum of contributions from many pinning sites, so the width is greater than that of the quantum flux states.

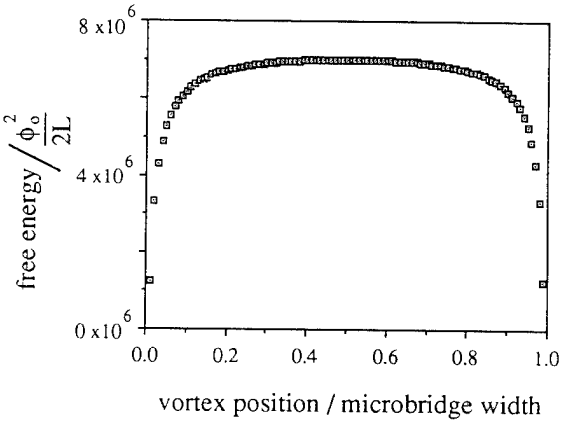

Figure 6. Energy of a vortex trapped in the microbridge in units of the energy of a flux quantum threading the loop.

Data

Method of Data Analysis

Data are taken in sets of 10 000 flux averages (Fig. 7). From each set, the data modulo ϕ_0 are binned into a histogram . A peak between quantum state values whose width is comparable to that of the quantum state peak indicates a strong pinning site. Although runs with such peaks have trapped flux, they are not used in the calculation of the trapping frequency because the identification of the quantum state peak versus the trapping peak is ambiguous.

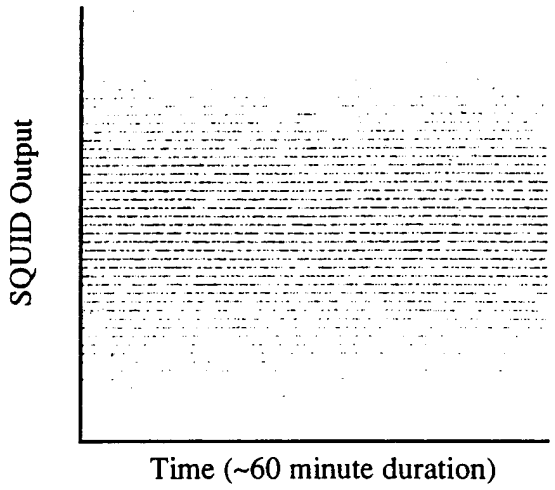

Figure 7. SQUID output.

In those runs with only shallow pinning sites, the number of trapped flux points is estimated using a statistical method known as Chauvenet's criterion.[4] The points on the histogram are fit to a Gaussian. Those points whose probability of occurance is less than 1/20 000 are eliminated, and the Gaussian is recalculated with the remaining points. This process is iterated until the standard deviation of the Gaussian changes by less than 0.1% between iterations. Those points that were rejected are considered trapped flux.

Diode Laser: 0.6 ms - 8 ms Optical Pulse Fall Times

Using the laser diode, we generated pulses with linear decay varying from 0.6 to 8 ms; the total pulse length was maintained at about 12 ms. Besides the quantum flux peak, there is no sharp peak in the distribution of trapped flux along the flux axis. This indicates the absence of any deep pinning sites. The distribution, shown in Fig. 8, has the broad shape, central maximum, and fall-off at the edges predicted for flux trapped in shallow pinning sites.

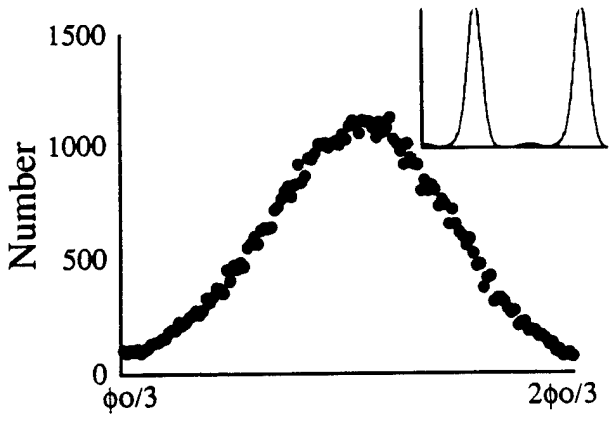

Figure 8. Spatial distribution of trapped flux. Inset: location and size of the trapped flux relative to the quantum state peak. The data modulo ϕ_0 have been plotted over two periods.

The frequency of trapped flux versus the fall time of the laser output is plotted in Fig. 9. The frequency does not correlate with the fall time over this time range.

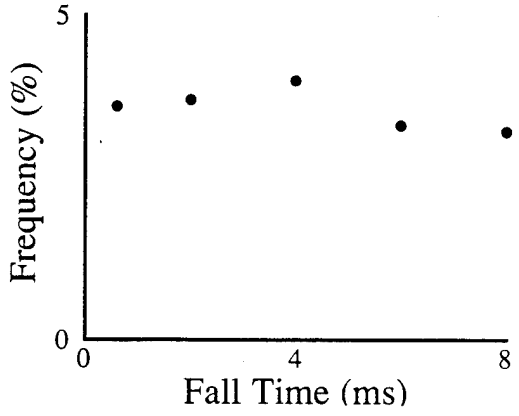

Figure 9. Frequency of trapped flux versus fall time, from 0.6 ms to 8 ms.

Diode Laser: 200 ns - 250 μs Optical Pulse Fall Times

In our next set of runs, we changed the chip and used a programmable pulse generator to modulate the diode laser. The optical pulse fall time was varied from 200 ns to 250 μs, with the total pulse length maintained at about 5 ms. The fall was again linear. For these data, we lengthened the averaging time and improved the antialiasing filtering.

Whereas the chip characterized in the previous section showed no evidence of deep pinning sites, this chip appears to have three. When the deep pinning sites are active, flux trapping increases dramatically. Frequent pinning occurs in at least one of these sites in two thirds of the runs, regardless of the fall time. Fig. 10 shows typical histograms of data modulo ϕ_0, taken at four different laser pulse fall times.

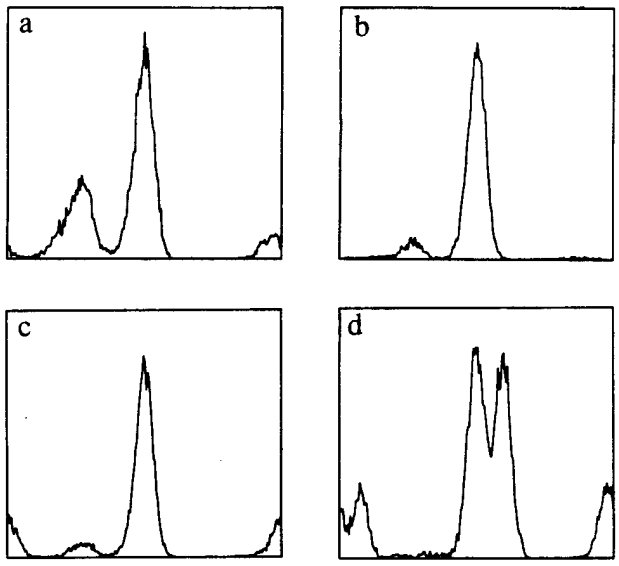

Figure 10. Histograms demonstrating deeply trapped flux in runs with a) 200 ns, b) 1.5 μs, c) 60 μs, and d) 250 μs optical pulse fall times. Half peaks on the sides of the graphs belong to the same pinning site, since the data are plotted modulo ϕ_0.

One third of the runs contained no evidence of strong pinning sites. With these runs, we calculated the frequency of trapped flux for the different pulse fall times and found no correlation (Fig. 11).

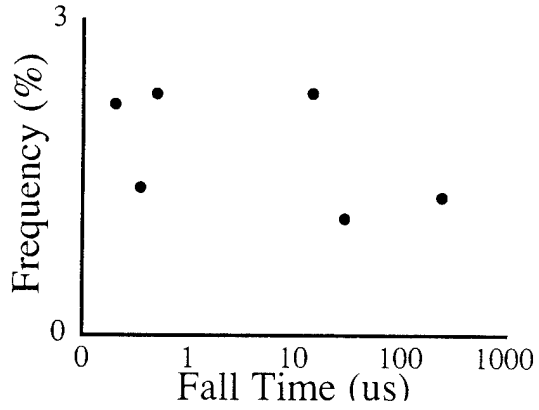

Figure 11. Frequency of trapped flux versus laser pulse fall time.

Nd:YAG Laser

We replaced the diode laser with a continuous wave (cw) Nd:YAG laser, leaving the rest of the system unchanged, and performed another set of runs. Unlike the laser diode system, the Nd:YAG system never trapped flux in the microbridge.

Noise Power Spectral Analysis

Using a photodiode, we compared the noise power spectra of the two lasers (operating in cw mode) over a 500 MHz bandwidth (Fig. 12). The periodic peaks in the noise power spectrum of the diode laser, appearing every 17.6 MHz, are probably etalon modes of the 5.5 m fiber attached to the laser. We believe that the increased noise starting at 200 MHz in the diode laser spectrum is due to relaxation oscillations in the laser.[5] Up to 200 MHz, the diode laser noise is 25% to 100% greater than the Nd:YAG laser noise. At 300 MHz, the diode laser noise is 5 to 25 times greater. It may increase further at frequencies above the 300 MHz bandwidth limit of the photodiode.

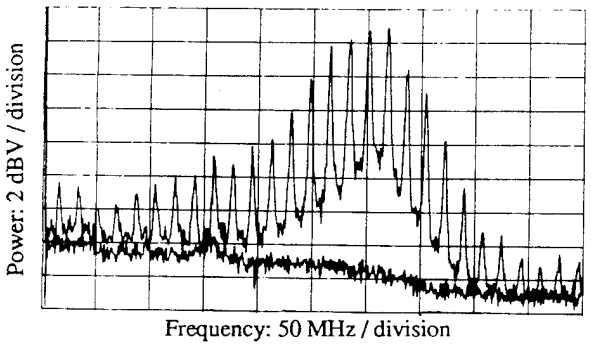

Figure 12. Noise power spectra of the diode (upper curve) and the Nd:YAG (lower curve) lasers.

The diode laser is noisier than the Nd:YAG laser on an oscilloscope of 200 MHz bandwidth (Fig 13). In fact, the noise power of the Nd:YAG laser is not significantly different from the photodiode "dark noise", the noise of the photodiode with no optical signal. The diode laser was studied further with an oscilloscope of 1 GHz bandwidth. The peak-to-peak dark noise is 35 (± 6) μW at this bandwidth. The noise power of the diode laser with the dark noise removed is shown in Tab. 1.

Table 1. Laser diode noise power, less photodiode dark noise

cw power (μW)	peak-to-peak noise (μW)
440	76 (± 16)
800	76 (± 16)
1250	60 (± 14)
2210	52 (± 18)

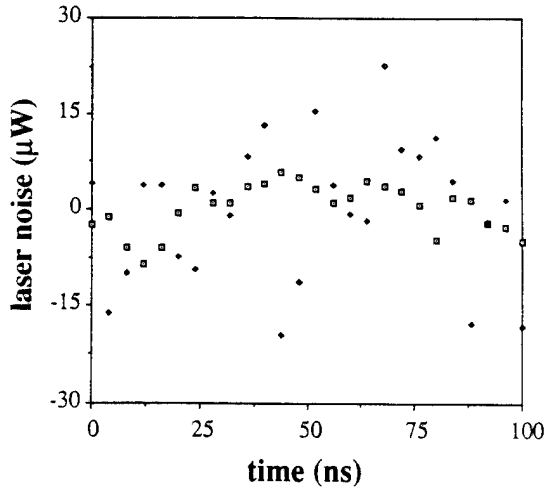

Figure 13. Oscilloscope traces of the diode (dots) and the Nd:YAG (squares) laser outputs at a 250 MHz sampling rate.

We believe that the increased noise at high frequency in the laser diode is a major factor in the incidence of trapped flux. This noise causes fluctuations of the laser intensity on the timescale of flux crossing the microbridge (about 2 ns). When the intensity decreases, it becomes more difficult for the vortex to move in the line, and it is likely to fall into a nearby pinning site.

Conclusion

We have determined that, in the time scale from 200 ns to 8 ms, the fall time of the laser pulse intensity does not affect the incidence of trapped flux in an optically switched microbridge. For shallow pinning sites, we have a model which correctly predicts the observed trapped flux distribution and relates the flux distribution to a spatial distribution.

We believe that high frequency noise from the laser diode causes flux trapping. Due to their high gain and small size, diode lasers are unusually susceptible both to relaxation oscillations and to reflections which result in etalon modes. We are now working on a method to reduce this noise.

Finally, we have shown that it is possible to have switching without trapped flux (using the shuttered Nd:YAG system) even with a chip with known deep pinning sites. We are confident that such switches can be used to reduce the level of 1/f noise in SQUID magnetometers.

Acknowledgements

The authors would like to thank E. Riis for helpful discussions about lasers. This material is based upon work supported by the National Science Foundation (G.S.P.). This work was funded in part by the Office of Naval Research, Contract #N00014-87-K-0135.

References

1. J. T. Anderson *et al.*, *Rev. Sci. Instrum.* 60 (1989) 202 and 209.
2. Charles E. Cunningham *et al.*, *Physica* **165** (1990) 113.
3. J. Pearl, *Applied Physics Letters* **5** (1964) 65.
4. H. D. Young: "Statistical Treatment of Experimental Data" (McGraw-Hill, New York, 1962), pp. 78-80.
5. Amnon Yariv: "Introduction to Optical Electronics" (Holt, Rinehart, and Winston, New York, 1971), pp. 147-153.

Vortex Pinning Force in a Superconducting Niobium Strip

George S. Park, Charles E. Cunningham,[a] and Blas Cabrera
Physics Department, Stanford University, Stanford, California 94305

Martin E. Huber[b]
Electromagnetic Technology Division, National Institute of Standards and Technology, Boulder, Colorado 80303
(Received 24 October 1991)

Using a SQUID-based technique, we measure the Lorentz force needed to depin a single trapped vortex in a superconducting Nb strip. The vortex is trapped by heating a portion of the strip above its critical temperature T_c with a laser pulse. Between 3.0 and 5.5 K, the pinning force obeys a power law $f_p = f_p(0)(1 - T/T_c)^n$, where $f_p(0) = (4.1 \pm 0.4) \times 10^{-4}$ N/m and $n = 1.9 \pm 0.1$. We have determined at a confidence level of 99.2% that we trap single vortices, rather than multiple vortices or vortex-antivortex pairs.

PACS numbers: 74.60.Ge, 74.75.+t

Recently, there has been much interest in the pinning forces on vortices in superconducting films. This interest stems from the importance of flux pinning for high critical current densities in high-temperature superconductor films, and because the presence of trapped magnetic flux affects the performance of low-temperature superconducting devices. Vortex trapping is not well understood from a theoretical standpoint, and much work has been done to try to measure the vortex pinning force and its temperature dependence. Allen and Claassen [1] used a magnetically coupled coil to induce and depin groups of vortices in a niobium film. Goldstein and Moulton [2] trapped vortices by heating a niobium film, and then observed their expulsion by a temperature gradient. Unfortunately, these and other [3,4] experiments dealt with groups of vortices, and so could not give a definitive value for the intrinsic pinning force on a single vortex. Hyun *et al.* [5] measured the single vortex pinning force using a diffraction method in a tunnel junction; however, the results apply only to "bent" vortices which penetrate just one strip in a cross-strip Josephson junction and exit through the insulator. In contrast to these experiments, we have devised a method to measure the pinning force of a single vortex in a simple superconducting strip.

A 20-nm-thick film of niobium is deposited on a 6.3 mm×6.3 mm silicon chip by dc magnetron sputtering. The film is plasma etched into two contact pads which are connected by a 2.2-μm-wide strip. Halfway between the pads, the strip is patterned into a zigzag meander of 5 μm pitch which occupies a square 85 μm on a side [Fig. 1(a)]. An optical fiber with a 50-μm core is aligned over the meander using a commercially available ruby ferrule which is epoxied to the chip. The niobium in the meander can be driven normal by sending 0.3 mW of 850-nm laser light down the fiber. This system is contained within a niobium cylinder and a high magnetic permeability shield which reduces the external field to less than 10^{-7} T.

We trap vortices in the meander using laser pulses. Initially, the chip is held at a temperature below the niobium's transition temperature. The laser is turned on, warming the meander into the normal state. When the laser is turned off, the entire meander usually cools into the superconducting state, and all magnetic flux is expelled out the sides of the strip. However, if the mode interference speckle pattern at the fiber output leaves a local "hot spot" during the turn-off, a vortex of magnetic flux may get trapped within the strip [6]. It is energetically favorable for the vortex to leave the strip, but the vortex can occupy a long-lived metastable state if the temperature of the chip is much lower than the critical temperature of the niobium film. Under these circumstances, we can study the vortex.

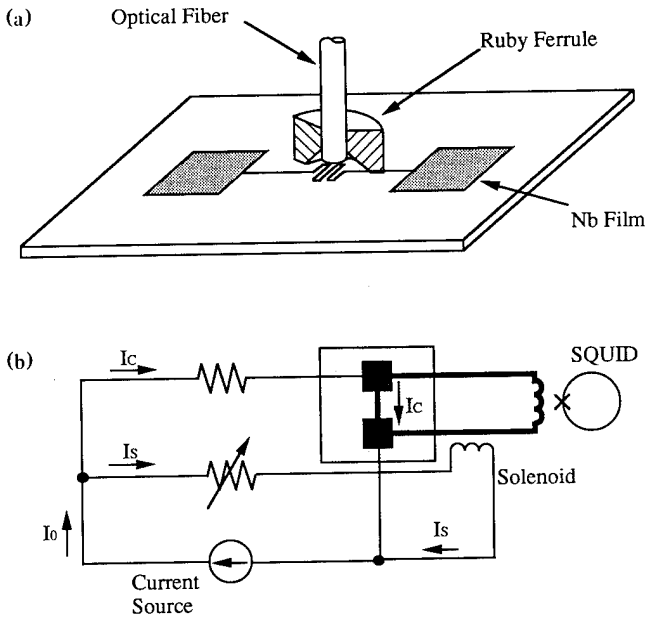

FIG. 1. (a) Laser switch chip. A simplified meander pattern has been drawn; the actual meander consists of eighteen lines. (b) Circuit schematic; heavy lines are superconducting.

The trapped vortex is detected using an rf SQUID (superconducting quantum interference device) magnetically coupled to a superconducting inductive loop which contains the thin strip [Fig. 1(b)]. Superconducting contact to the chip is made by pressing dimpled niobium foils against the contact pads. Niobium wires are spot welded to the foils and are connected to the SQUID's input coil. One wire passes through a toroidal solenoid which is used to couple magnetic flux to the loop. Since the entire loop is superconducting, integration of the Ginzburg-Landau equation around the loop forces the magnetic flux Φ inside the loop to be some integer multiple of the flux quantum $\Phi_0 = h/2e$:

$$\Phi + \mu_0 \lambda^2 \oint \mathbf{j}_s \cdot d\mathbf{l} = n\Phi_0 , \quad (1)$$

where j_s is the supercurrent density, n is an integer, and λ is the penetration depth of the superconductor. The line integral traces the superconducting loop through the strip, foils, wires, and input coil. Except for the short length at the strip, the loop is comprised of elements thick compared with the penetration depth; thus, since the supercurrent density vanishes many penetration depths inside of these elements, the integral term in the equation is small. The presence of a vortex changes the flux quantization condition because line integral paths which enclose the vortex satisfy Eq. (1) with n becoming $n \pm 1$ with respect to paths that do not enclose the vortex. If the vortex is a distance d from the edge of a strip of width w, and the integration path is a distance x from the edge of the strip when it passes the vortex, then

$$\Phi + \mu_0 \lambda^2 \oint \mathbf{j}_s \cdot d\mathbf{l} = \begin{cases} n\Phi_0 & (0 < x < d), \\ (n \pm 1)\Phi_0 & (d < x < w). \end{cases} \quad (2)$$

Referring to Fig. 2(a), integration paths which pass "above" the vortex will couple to the vortex flux, while paths which pass "below" the vortex will not. Because the SQUID output voltage is proportional to the total circulating current, we know that a vortex is trapped in the strip when the SQUID output is between quantum values. Qualitatively, the situation can be considered in terms of a vortex moving from one side of the strip to the other, continuously varying the value of the enclosed flux from n to $n \pm 1$. Since it is proportional to the enclosed flux, the total current will also vary continuously from one quantum value to the other. If the vortex remains within the strip, the total current, and hence the SQUID response, will remain between the two quantum values.

Once we have induced and detected a pinned vortex, we apply a Lorentz force to it by slowly ramping a current through the strip. The current I_0 flows through an adjustable current divider, so that I_c is sent to the chip by a pair of Manganin wires spot welded to the niobium foils, and I_s is sent to the solenoid [Fig. 1(b)]. At the chip, the current I_c divides: A fraction flows through the strip and the rest flows through the SQUID's input coil.

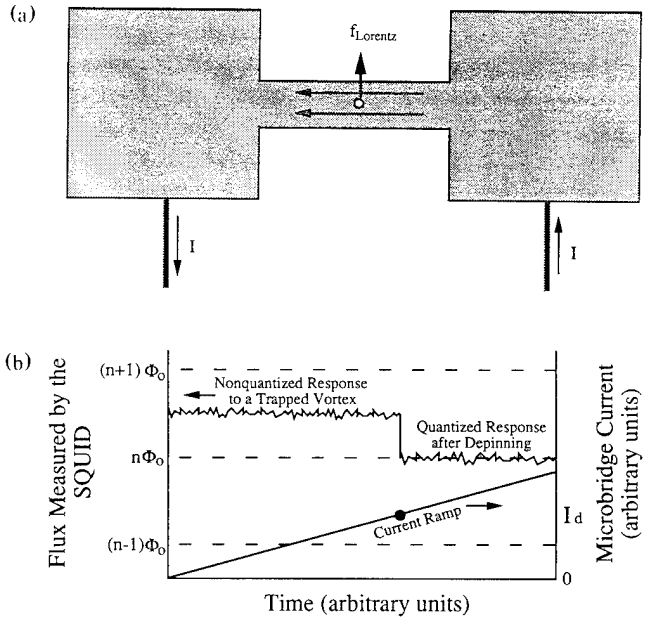

FIG. 2. (a) Current produces a Lorentz force on vortex. (b) SQUID response to vortex depinning by a current ramp through the chip (simulation).

The current divider is adjusted so that the solenoid current induces a shielding current in the superconducting loop that exactly cancels the portion of I_c going through the SQUID input coil. This circulating current adds to the current in the strip, so that the strip current is I_c. Experimentally, we were able to drive over 10 mA through the strip before nonlinearities (most likely, changes in the resistance due to Joule heating in the leads and the toroidal windings) upset the balance of currents.

As we ramp the current through the strip, the Lorentz force on the vortex increases until it equals the pinning force [Fig. 2(a)]. At this depinning current I_d, the vortex "pops" out of the strip, and the event is recorded by the SQUID [Fig. 2(b)]. Assuming the current density in the strip is uniform, the depinning current density $J_d = I_d/wt$, where w and t are the width and thickness of the strip, and the depinning force is $f_p = J_d \Phi_0$.

Chip temperatures above 4.2 K are achieved by raising the probe partly above the liquid-He bath. Chip temperatures below 4.2 K are achieved by pumping the liquid-He bath. The temperature is measured by a carbon resistor in thermal contact with the chip. These techniques are used in a separate four-terminal experiment to determine our niobium sample's T_c (at the experimental ambient magnetic field of < 0.1 μT).

In a series of runs, we induce and depin single vortices at temperatures ranging from 3 to 5.5 K. Below 3 K, the SQUID no longer operates; above 5.5 K, thermal fluctuations depin trapped vortices. The data are shown in Fig. 3. The temperature dependence is clearly visible, but the depinning current for different trapping sites varies by as much as a factor of 2 at any given temperature.

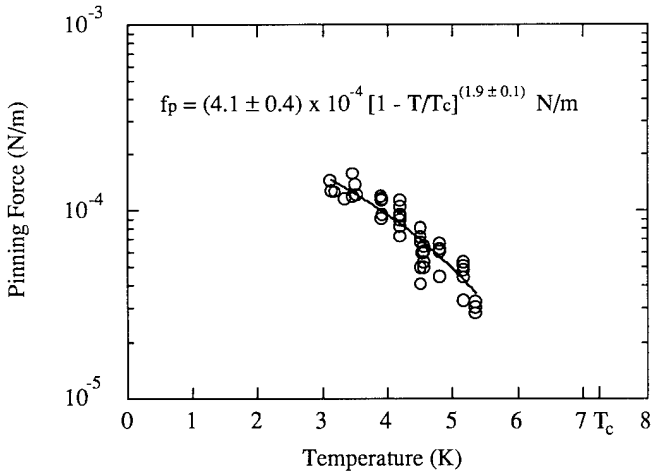

FIG. 3. Pinning force measurements with best fit by empirical model.

We fitted our data by the empirical power law $f_p = f_p(0)(1 - T/T_c)^n$, where $T_c = 7.35$ K. The best fit parameters were $f_p(0) = (4.1 \pm 0.4) \times 10^{-4}$ N/m and $n = 1.9 \pm 0.1$. Because the details of the pinning mechanism are not known, there is at present no theory to predict values for $f_p(0)$ or n. However, our value for $f_p(0)$ is in general agreement with previous measurements. For example, Allen and Claassen [1] obtained $f_p(0)$ values of 10^{-6} to 10^{-5} N/m for niobium films which were specially prepared to minimize the pinning force. Since our films were not similarly prepared, we would expect and have observed a higher value for the pinning force. The measurement of Hyun *et al.* yielded an exponent of 1.5 [5], whereas the niobium film measurement made by Allen and Claassen yielded exponents of 2.7 ± 0.2 and 3.5 ± 0.3, depending on the film tested [1]. Our measured exponent (1.9) lies between these values.

Occasionally, we see two depinning events during a single current ramp. This behavior is caused by a single vortex that is depinned from one site, trapped in a second site, and then depinned from the second site. We can rule out a signal resulting from two vortices for the following reason. If we had two vortices, we would expect them to have the same polarity (into or out of the film) half the time, in which case a double depinning would cause a flux change of more than one Φ_0. In seven double depinning events, we never saw a signal larger than Φ_0, so the probability that these events result from two vortices is $< 0.8\%$. Hence, we believe that each event is a single vortex which is depinned twice, rather than multiple vortices or vortex-antivortex pairs. The second pinning site must have a stronger pinning force and must be closer to the exiting edge of the strip than the first site. These events occur at various temperatures and positions of the vortex in the strip.

Our technique measures not only the pinning force, but also the pinning location. The SQUID response to a trapped vortex is approximately proportional to its position across the width of the strip [7]. During the experiment, we observed vortex trapping in sites spanning the entire width; however, we studied only those vortices in the middle 60% of the strip. Through this selection, we were confident that we were looking at trapped vortex states, rather than fully superconducting states with biased noise.

We tried to correlate the single vortex pinning force with the location of the vortex. Because of shielding effects, the current density near the edge of the strip is about 10% greater than near the center. Thus, for equal pinning potentials, we would expect to measure up to a 10% difference in the pinning force depending on the location of the trapping site. However, the pinning force for different sites varies by as much as a factor of 2, dwarfing the effect of the small nonuniformity in current density. In our statistically small number of runs, we did not see any correlation between pinning force and location. Furthermore, we have seen double depinning events where the initial pinning site was near the center and the second site near the edge. As stated before, this situation implies that the second site had a deeper potential than the first, even after accounting for the effect of the increased current density.

In conclusion, we have developed a method to measure the pinning force of single trapped vortices in our niobium strip over a substantial temperature range. This arrangement avoids the statistical uncertainties of multiple vortex methods as well as the complicated geometries of Josephson cross-strip methods. In the future, we plan to apply our technique to other materials.

This work has been supported in part by Office of Naval Research Contract No. N00014-90-J-1528. This experiment is based in part upon work performed under a National Research Council–National Institute of Standards and Technology Associateship (M.E.H.) and a National Science Foundation Fellowship (G.S.P.).

---

[a]Current address: Laboratory for Experimental Astrophysics, Lawrence Livermore National Laboratory, Livermore, CA 94550.

[b]Current address: Physics Department, University of Colorado, Denver, CO 80217.

[1] L. H. Allen and J. H. Claassen, Phys. Rev. B **39**, 2054 (1989).

[2] M. J. Goldstein and W. G. Moulton, Phys. Rev. B **40**, 8714 (1989).

[3] J. Mannhart, J. Bosch, R. Gross, and R. P. Huebener, Phys. Lett. A **122**, 439 (1987).

[4] B. M. Lairson, J. Z. Sun, T. H. Geballe, M. R. Beasley, and J. C. Bravman, Phys. Rev. B **43**, 10405 (1991).

[5] O. B. Hyun, D. K. Finnemore, L. Schwartzkopf, and J. R. Clem, Phys. Rev. Lett. **58**, 599 (1987).

[6] G. S. Park, C. E. Cunningham, B. Cabrera, and M. E. Huber (to be published).

[7] G. S. Park, C. E. Cunningham, B. Cabrera, and M. E. Huber, IEEE Trans. Mag. **27**, 3021 (1991).